NONLINEAR FLUTTER ANALYSIS OF A MISSILE WITH NONLINEARITY AND HYSTERESIS

Ariel Drachinsky[1]

[1] Research associate,
Rafael- Advanced Defense Systems LTD.
arield@rafael.co.il, arikdra@gmail.com

Nomenclature

A	= Linear dynamic matrix (contains the structural and aerodynamic model)
AIC	= Aerodynamic influence coefficient matrix
AoA	= angle of attack
B_{NL}	= input distribution matrix
C	=damping matrix
C_{LU}	=Matrix that connects modal displacements to outputs into the control loop
D	=Matrix that distributes the direct force effect on the outputs of the system
DOE	=Design of experiment
DLM	=Doublet lattice method
EOM	=Equation of motion
F	=Force vector
F_a	=Aerodynamic force vector
FD	=Frequency domain
FE	=Finite element
FEM	=Finite element model
FFT	=Fast Fourier transformation
FRF	=Frequency response function
G	=Spline matrix between structural and aerodynamic grids
GC	=Modal damping matrix
GF_a	=Aerodynamic modal force vector
GF_{ext}	=External forces converted to modal coordinates
GK	=Modal stiffness matrix
GM	=Modal mass matrix
GVT	=Ground vibration test
$IFFT$	=Inverse Fast Fourier transformation
IOM	=Increased order model
K	=Stiffness matrix
M	=Mass matrix
M_{hinge}	=hinge moment
M_{hinge_max}	=Moment limit of the slider element
M_0	=hinge moment due to initial angle of attack
NL	=Non-linear
q	=Dynamic pressure
u_{NL}	= Vector of inputs from the nonlinear block
t_{off}	=time at which the fictitious stabilizing spring is turned on
v	=Airflow velocity
X_{LU}	= FRF of the linear system to unit inputs from the non-linear block
X_L	= Vector of linear contribution to displacements
X_{NL}	= Vector of non-linear contribution to displacements
x_t	= Vector of total modal displacements
y_L	=outputs of the linear block (or inputs to the non-linear block)
$Y_{LU}(i\omega)$	=FRF outputs of to the NL block to inputs of the NL block
$Y_{LU}(t)$	=Impulse response of outputs of to the NL block to inputs of the NL block
y_{NL}	=outputs of the non-linear block (or inputs to the linear block)

θ_{fin} =Fin angle
θ_0 =Initial fin angle (due to angle of attack)
ξ =Modal displacement
ϕ =Modal matrix in structural grids
ϕ_a =Modal matrix in aerodynamic grids
ω =Frequency [rad/sec]

Keywords: aeroelasticity, flutter, hysteresis, structural dynamics, IOM method

Abstract: This paper presents a computational and experimental study of the nonlinear aeroelastic response of a missile containing softening and hysteresis in the actuator of its fin. The aim of the work was to study the effect of the nonlinearity and the hysteresis on the dynamic stability of the configuration, and on the type of the obtained instability, mainly focusing on the question whether the oscillations would converge to a limit cycle oscillation (LCO) or diverge.
The mathematical model is based on the Increased Order Model (IOM) method, implemented by the DYNRESP software, for the nonlinear solution. The structural model is a modal model calibrated vs GVT tests, and the aerodynamic model is based on an unsteady panel model. The nonlinearity is based on static measurements of the actuator stiffness, and is modeled in the study as an external non-linear feedback loop for the main linear block.
The effect of the nonlinearity and softening and hysteresis on the onset velocity is studied along with the effect of the amplitude of initial conditions and an initial static angle of attack. Finally, some of the trends obtained in the simulations are shown in wind tunnel test results.

1 INTRODUCTION

In recent years, performance demands from aerospace structures grow increasingly. This leads to lighter configurations with larger aspect ratio wings. Lower cost demands lead to the use of cheaper materials and production technologies; while on the other hand, the time to market shortens. These trends increase the need for more accurate simulations which can predict complicated phenomena, and can be used for DOE analysis, for optimization and decrease the amount of high cost flight tests performed.
Numerous studies examine the effect of non-linear stiffness and damping (eg.[1],[2], [3], [4]), few of them deal with missile configurations and even fewer assess the effect of hysteresis on the aeroelastic response of structures. In many cases, the non-linearity is accompanied by a hysteresis in the structural response. These effects can result from preloaded joints with frictional connections, from non-linear material properties in polymers, from plastic strains in metallic structures etc. Reference.[5] analyzed a 2D airfoil with simplified hysteresis model and hardening effect, with qasy steady aerodynamics. Reference [6] analyzed the effects of hysteresis on aircraft aeroelastic response using linearization, based on the harmonic balance method. Reference [7] studies hysteresis in the context of flutter suppression using a tuned mass damper..
The current study presents a non-linear flutter analysis of a generic missile having nonlinear actuator-stiffness in of the control surface. The nonlinearity consists of structural softening and hysteresis. The goal of the study is to derive a computational method to model and analyze the effect of hysteresis on the aeroelastic response of the structure, and to study the effect of the hysteresis on the overall aeroelastic behavior of the system. A time marching analysis is conducted in modal coordinates, using the "Increased Order Model" (IOM) method, implemented in the Dynresp software. The IOM method has proven to be an efficient tool for modeling and analysis of aeroelastic systems with nonlinearities in its control systems, structure or aerodynamics ([8], [9], [10]). The IOM method is based on dividing the

model into a frequency-domain linear block and a time-domain nonlinear feedback block. The aerodynamic model, in this work, is based on the panel model utilized in the ZAERO code. The structural model consists of two parts: a linear FEM, built in Ansys and calibrated versus GVT results, and a nonlinear actuator model. The non-linear actuator stiffness is based on a static structural experiment and is modeled using Maxwell's slip model, which represents a softening-hysteresis system using a finite number of slider-spring elements. The basic-linearized model and the aerodynamic model are imported into the Dynresp software, and the non-linear actuator model, is modeled inside the Dynresp code as a nonlinear feedback loop.

2 MATHEMATICAL MODEL

2.1 Studied configuration

The studied configuration is a missile with four folding wings and four folding fins. The wings are deployed during ejection and are fixed via a locking mechanism. The fins are deployed in a similar way. The main difference between the wings and fins is their torsional rigidity. Unlike the wings that are fixed after deployment, the fins are connected to a servo unit. This connection is relatively soft in terms of torsion and bending of the actuator and the servo structure. These stiffness parameters were measured in a static test, and the actuator stiffness was found to be highly non-linear, containing a softening nonlinearity and a hysteresis. The visualizations in the paper are presented on a similar configuration to the one in the study. Results from the actuator stiffness test are presented in Figure 1.

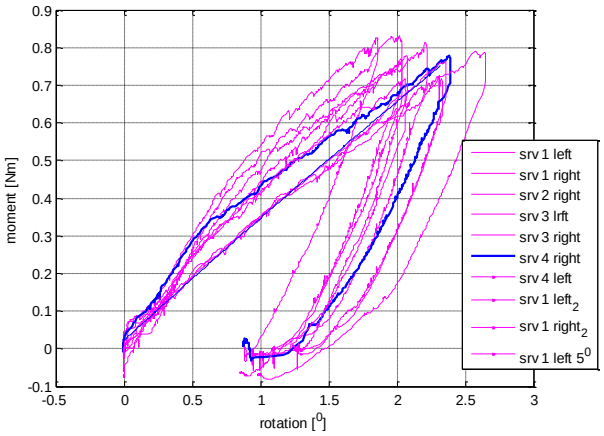

Figure 1: Results from stiffness tests on actuators. The blue line is the result used for the simulations.

2.2 The IOM method

The IOM method is based on a main linear block with the nonlinear effects modeled as a NL feed-back loop [9]. The linear core model is represented in FD, and the NL system operates in time domain, where the data transfer between them is done using FFT and IFFT. The linear model is given in FD by

$$\left[A(i\omega)\right]\{x_t\} = \left[B_{NL}(i\omega)\right]\{u_{NL}\} + \{GF_{ext}(i\omega)\} \tag{1}$$

Where $\{x_t\}$ is a vector of modal displacements, $\{u_{NL}\}$ is a vector of inputs from the nonlinear block, A is the dynamic matrix (contains the structural and aerodynamic models), $[B_{NL}]$ is the input distribution matrix. In case of direct force feedback, it is a matrix of the modal effect of the input forces. GF_{ext} are the external forces converted to modal coordinates and transferred to the FD via FFT.

The solution is based on separating the effect of the linear system and the response to the NL feedback loop;

$$\{x_t\} = \{x_L\} + \{x_{NL}\} \tag{2}$$

$$\{x_L\} = \left[A(i\omega)\right]^{-1} \cdot \{GF_{ext}(i\omega)\} \tag{3}$$

$$\{x_{NL}\} = \left[A(i\omega)\right]^{-1} \cdot \left[B_{NL}(i\omega)\right]\{u_{NL}(i\omega)\} \tag{4}$$

The IOM is implemented in a five-stage procedure

1. First the response of the linear baseline model to the external excitation is evaluated in frequency domain.

$$\{x_L\} = \left[A(i\omega)\right]^{-1} \cdot \{GF_{ext}(i\omega)\} \tag{4}$$

   The outputs (due to external excitation) of the linear block, which are the inputs of the NL block are evaluated

$$\{y_L\} = \left[C_{LU}(i\omega)\right] \cdot \{x_L(i\omega)\} + \left[D(i\omega)\right] \cdot \{GF_{ext}(i\omega)\} \tag{4}$$

   C is a modal matrix that connects the modal displacements to outputs into the control loop, in physical coordinates. D represents direct force effect (relevant only in case the of acceleration outputs)

2. Then the FRF of the linear system to unit inputs from the non-linear block is evaluated.

$$\{x_{NL}\} = \underbrace{\left[A(i\omega)\right]^{-1} \cdot \left[B_{NL}(i\omega)\right]}_{[X_{LU}]}\{u_{NL}\} \tag{4}$$

   Therefore, the FRF outputs of to the NL block to inputs of the NL block are

$$\begin{aligned} \{y_L\} &= \left[C_{LU}(i\omega)\right] \cdot \{x_{NL}(i\omega)\} + \left[D(i\omega)\right] \cdot \{u_{NL}(i\omega)\} = \\ &= \underbrace{\left[C_{LU}(i\omega)\right] \cdot \left[A(i\omega)\right]^{-1} \cdot \left[B_{NL}(i\omega)\right] + \left[D(i\omega)\right]}_{[Y_{LU}(i\omega)]} \cdot \{u_{NL}(i\omega)\} \end{aligned} \tag{4}$$

3. The third step is evaluation of the time domain response of the linear system to the external excitation, and the time domain response of the outputs to the NL blocks to unit inputs from the NL block by IFFT of the results of $\{y_L\}$ and $\{y_{LU}\}$.

4. The fourth step is evaluation of the outputs of the NL block using a time marching NL solution based on the inputs from the NL block and on a convolution of the outputs on the NL block and the time response of the linear system to them.

$$\{y_{NL}(t)\} = \{y_L(t)\} + \int_0^t [Y_{LU}(t)]\{u_{NL}(\tau)\} \tag{4}$$

5. Finally, the outputs of the NL block are converted to frequency domain by FFT, which enables a frequency domain calculation of the actual response of the system.

$$\begin{aligned} \{x_{NL}\} &= [A(i\omega)]^{-1} \cdot [B_{NL}(i\omega)]\{u_{NL}(i\omega)\} \\ \{x_t\} &= \{x_L(i\omega)\} + \{x_{NL}(i\omega)\} \end{aligned} \tag{4}$$

The result vector is then transferred to time domain via IFFT.

2.3 Structural model

The linear, structural equation of motion is given by:

$$[M]\{\ddot{X}\} + [C]\{\dot{X}\} + [K]\{X\} = \{F\} \tag{4}$$

where [K] and [M] are the structural stiffness and mass matrices, in our case evaluated using ANSYS finite element code. C is the damping matrix which is usually added in the modal system as modal damping. {F} is the forces vector. The solution is based on a modal decomposition, assuming the displacement vector in physical coordinates can be described as a linear superposition of the structures mode shapes.

$$\{X\} = [\phi] \cdot \{\xi\} \tag{4}$$

$$[\phi] = [\{\phi_1\} \quad \{\phi_2\} \quad \cdots] \tag{4}$$

Where [ϕ] is the modes matrix, in which each column is a mode in physical coordinates, and {ξ} is a vector of modal displacements.
After substitution and pre-multiplication by the modal matrix [ϕ], the EOM in modal coordinates is obtained:

$$[GM]\{\ddot{\xi}\} + [GC]\{\xi\} + [GK]\{\xi\} = \{GF\} \tag{4}$$

where

$$[GM] = [\phi]^t [M][\phi] \tag{50}$$

$$[GK] = [\phi]^t [k][\phi] \tag{51}$$

$$\{GF\} = [\phi]^t \{F\} \tag{52}$$

An eigenvalue problem, neglecting the structural damping and the aerodynamic forcing term, is solved in the FE code. The solution yields generalized mass and stiffness matrices, the

Eigen frequencies, and the mode shapes. The solution is then conducted on the reduced modal system.
The baseline structural model is a finite element model (FEM), created in Ansys. The body of the missile is represented by beam elements, representing its flexural stiffness. The fins are modeled with shell elements, with varying thickness. Two rotational springs represent connection regions in the body. The stiffness of the springs is calibrated based on a GVT test. In order to connect the fins at the location of the actuator, rigid beams are connected between the body and the location of the axis. The fins are connected to the tip of the rigid beams using spring elements, representing the bending and torsion stiffness of the actuator. A similar model is presented in Figure 2 for the sake of visualization.

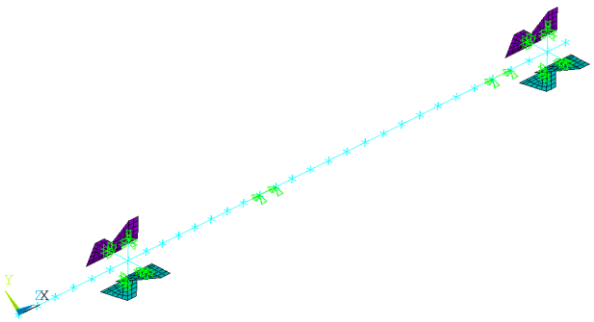

Figure 2: Structural model of a similar configuration

The non-linear structural response is achieved by a fictitious, nonlinear control loop, that uses the fin rotations as an input and applies hinge moments as an output. The specifics on the nonlinear model are described in section 2.5.
the nonlinearity in the model results from the actuator of the fins. This is also the main component responsible for the torsional mode of the fins. The stiffness of the fins is not identical, and for simplicity, only the fin with the softest actuator (which is the fin that flutters), is modeled nonlinearly.
The bending stiffness of the fins and body are calibrated versus GVT tests. The body is calibrated by changing the stiffness of the connector-springs. The bending stiffness of the fins is calibrated through the spring element at the root of the fin. The torsional stiffness of the fins is calibrated versus the static stiffness tests conducted on the actuator. Since the actuator is nonlinear, the baseline model is linearized about the initial stiffness, near zero torsion.

2.3.1 Structural model modifications using fictitious masses

It has been shown (eg [11], [12]) that normal modes, obtained from a given model, can be used to sufficiently predict the response of a model with altered stiffness and mass parameters, and to predict the response of the structure to external and internal loads. However, if large local stiffness changes are to be made, or large local loads are to be applied (such as local fin stiffness or force), the model would require a large number of modes to catch the correct response. Alternatively, large fictitious masses can be used to create modes that represent the local desired phenomena. It has been shown in previous studies (eg. [12]), that modification of the model with large fictitious masses yields good accuracy of the model under a wide range of local structural changes and under local forces. The fictitious masses are removed in the actual simulation but the mode shapes would now contain local modes that represent the desired effect. In addition to the fictitious mass, the stiffness of the fin is reduced. This spring is replaced by the non-linear element in the actual simulation

The accuracy of the model is examined by comparing the eigenfrequencies of the baseline model to those of the modified model, obtained after the fictitious masses are removed using the equations below, and conducting an external modal analysis using the modified and fixed modal model.

$$\omega_{fixed} = eig\left(GK_{fixed}, GM_{fixed}\right) \tag{50}$$

$$GK_{fixed} = \left[GK_{\text{modified}}\right] + \left[\phi\right]^{T} \cdot \left[\Delta K\right] \cdot \left[\phi\right] \tag{51}$$

$$GM_{fixed} = \left[GM_{\text{modified}}\right] + \left[\phi\right]^{T} \cdot \left[\Delta M\right] \cdot \left[\phi\right] \tag{52}$$

ΔK and ΔM are matrices containing the additional stiffness and mass in the degrees of freedom of the actuator.
The comparison between the different models is presented in Table 1. It can be seen that the fictitious mass has only a local effect on the torsion mode of the fin and has little effect on the other structural modes. In addition, it is seen that adding back the stiffness and mass with the modified mode set, yields similar frequencies, thus indicating that the modified model is accurate.

Table 1 modal model comparison between the modified models (the frequencies are normalized)

Mode	**baseline**	**Modified (fictitious mass + reduced stiffness)**	**modified and fixed**
Fin 1 in plane bending	**0.595**	0.595	0.595
Fin 2 in plane bending	**0.596**	0.596	0.596
Fin 3 in plane bending	**0.596**	0.596	0.596
Fin 4 in plane bending	**0.600**	0.600	0.600
Wing 1 bending	**0.737**	0.737	0.737
Wing 2 bending	**0.748**	0.748	0.748
Wing 3 bending	**0.753**	0.753	0.753
Wing 4 bending	**0.767**	0.767	0.767
Fin 1 bending	**0.782**	0.782	0.782
Fin 2 bending	**0.816**	0.817	0.816
Fin 3 bending	**0.863**	0.865	0.864
Fin 4 bending	**0.912**	0.934	0.919
Body pitch bending	**1.158**	1.159	1.158
Body yaw bending	**1.261**	1.261	1.261
Fin 4 torsion	**1.369**	0.004	1.374
Fin 2 torsion	**1.642**	1.635	1.635
Fin 1 torsion	**1.681**	1.672	1.672
Fin 3 torsion	**1.691**	1.683	1.683

2.4 Aerodynamic model

The aerodynamic forces, in modal coordinates are given by

$$\{GF_a\} = [\phi_a]^t \{F_a\} \tag{52}$$

Were $[\phi_a]$ is a matrix of the modal displacements in the aerodynamic grid and F_a is the aerodynamic force vector.
The aerodynamic-force vector can be decomposed into a static, rigid component (resulting from the cross-section geometry and angles of attack) and an elastic component (resulting from the structural deflections and their time derivatives). The rigid forces have no effect on the stability analysis (in the linear region), and they can be ignored in the stability (flutter) solution. Their nonlinear effect is studied in chapter 0 and 3.5.

$$\{F_a\} = \cancel{\{F_{a0}\}} + \{F_a(X)\} + \{F_a(\dot{X})\} + \{F_a(\ddot{X})\} \tag{52}$$

The generalized aerodynamic forces are evaluated in frequency domain in the aeroelastic code (ZAERO), which uses an unsteady panel model (Zona-6). The generalized forces are given as a function of the modal displacements. They are evaluated per reduced-frequency as:

$$\{GF_A(i\omega)\} = [\phi_a]^T \, q \cdot [AIC(i\omega)][\phi_a]\{\xi\} \tag{52}$$

The fins and body are modeled with CAERO7 and Pbody7 element, respectively. The data between the FEM and the aerodynamic model is transferred via spline routines, embedded in the Zaero software. The resultant model is expressed with frequency dependant, complex modal stiffness/damping matrixes

$$\{Q_{HH}(i\omega)\} = [\phi]^T [G]^T \, q \cdot [AIC(i\omega)][G][\phi]\{\xi\} \tag{52}$$

Where [G] is the spline matrix, that converts the modes from the structural grfd to the aerodynamic grid. [AIC] is the aerodynamic influence coefficient matrix (product of ZONA 6 method), and q is the dynamic pressure.
For the sake of representation, a similar model to the model in the study is presented in Figure 3.
The linear system in frequency domain, can then be represented by

$$[A(i\omega)] = -\omega^2 [GM_{fixed}] + i\omega [GC_{\text{modal}}] + [GK_{fixed}] + q_d \cdot \{Q_{HH}(i\omega)\} \tag{52}$$

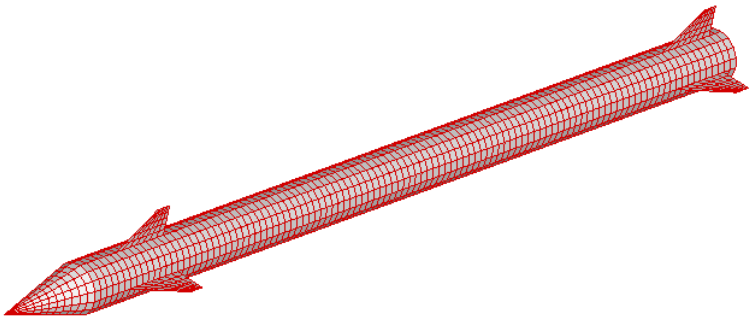

Figure 3: Aerodynamic model of a similar configuration

2.5 Non-linear block model

Since the IOM method operates in the frequency domain and uses FFT to pass between time and frequency domain, all the structural response must decay at the end of the simulation (repeatability assumption of the FFT). Since the simulation is of a non-linear flutter, this is clearly not the case. Therefore, the simulation is divided into two time zones. the first one is the actual simulation whereas the second one is a time frame in which the model is stabilized using a fictitious spring element that causes the response to decay. In addition, the main linear block must be stable for the initial linear simulation to converge (part of the IOM algorithm). Therefore, the fictitious spring should be applied on the linear model.

The following demands are achieved with the non-linear system presented in Figure 4. The linear core of the system is the plant model with reduction of the fictitious mass described in section 2.3.1 (using “conm” element), and addition of a fictitious spring (using “celas” element). The linear block is connected to a “control system” with the rotations as the output, and the fin moments as input. Besides the actual actuator nonlinearity, it contains a switch element that at a certain time “turns off” the whole non-linear block and lets the system decay to zero. It contains a NL gain element that applies an opposite force to the linear fictitious spring, thus canceling its effect in the first-time zone of the simulation. The result is a model that has the desired non-linearity in the first time-zone, is stable in the second, and has a stable linear core. This system (without the actual physical non-linearity) is presented in Figure 4, and is referred to, in the upcoming chapters as the NL plant.

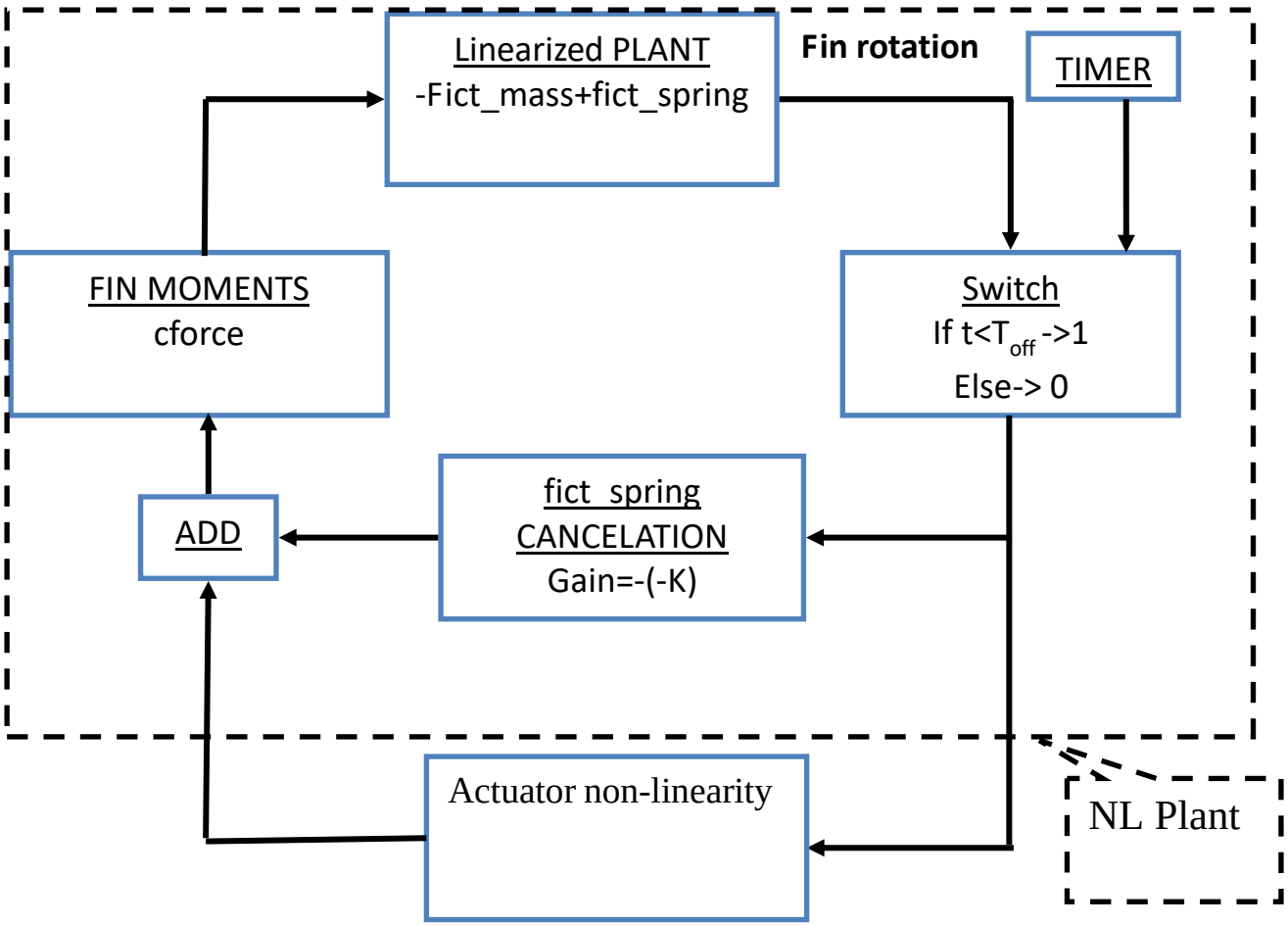

Figure 4: Block diagram of the NL plant system (dynamic system with necessary IOM method modifications)

2.5.1 Softening Nonlinearity

A softening nonlinearity (without hysteresis) was modeled using dynresp's NLGAIN command, which reflects a nonlinear control gain. The input is the hinge rotation, and the output is the hinge moment,

$$M = Gain\left(\theta_{fin}\right)\cdot\theta_{fin} \tag{52}$$

where, Gain(θ) is supplied in a tabular form and an interpulation is used between the given values.
The implementation of the nonlinear softening-only model in the overall model is presented in the block diagram in Figure 5

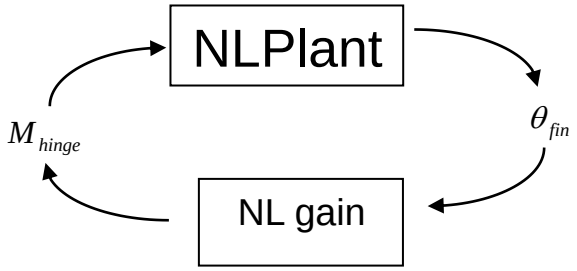

Figure 5: Block diagram of the softening NL model

2.5.2 Hysteresis

A various number of modeling techniques can be found in the literature. Some of them are well summarized in [13]. In the current study, The hysteresis was modeled using a Maxwell's slip model [13], where the hysteresis is modeled with a multitude on slider-spring elements connected parallelly. A single slider-spring element formulation yields a bi-linear hysteresis behavior. A multitude of slider-spring elements can be designed to yield a mode complex behavior. As the slider element is not implemented inside the Dynresp software, it was implemented using a user's function. The mathematical formulation of the slider-spring element was formulated in incremental form

$$d\theta_{fin} = \theta_{fin}(i) - \theta_{fin}(i-1)$$

$$\begin{cases} M_{hinge}(i) = M_{hinge}(i-1) + k \cdot d\theta_{fin} & , \left| M_{hinge}(i-1) + k \cdot d\theta_{fin} \right| < M_{hinge\_\max} \\ M_{hinge}(i) = sign\left(d\theta_{fin}\right) \cdot M_{hinge\_\max} & , \left| M_{hinge}(i-1) + k \cdot d\theta_{fin} \right| > M_{hinge\_\max} \end{cases} \quad (52)$$

visualizations of the slider-spring element and its behavior, for a case of a single element or multiple elements are presented in Figure 6.

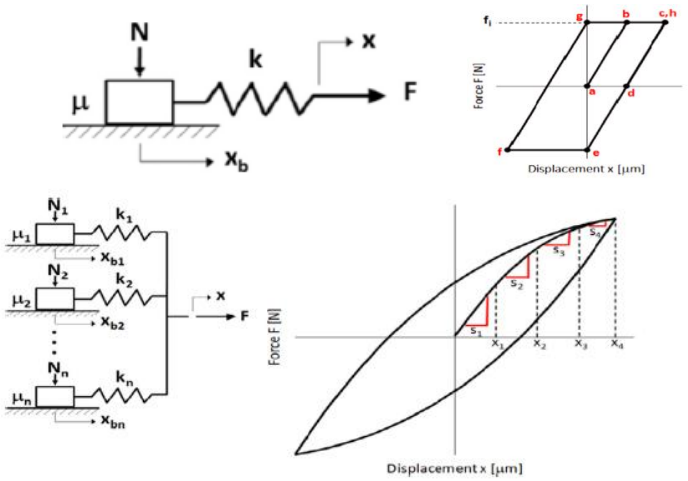

Figure 6: Visual representation of Maxwell's slip theory. Single slider- top, multiple sliders- bottom

A comparison between measured data and the nonlinear models (softening and softening + hysteresis) is presented in Figure 7, showing good agreement between the structural test, the "nonlinearity-only" model and the "nonlinearity and hysteresis" model.

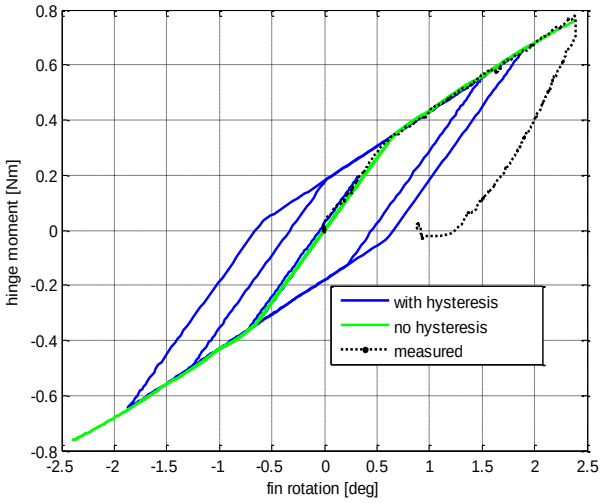

Figure 7: Comparison of obtained models to experimental results

The implementation of the hysteresis model in the overall model is presented in the block diagram in Figure 8.

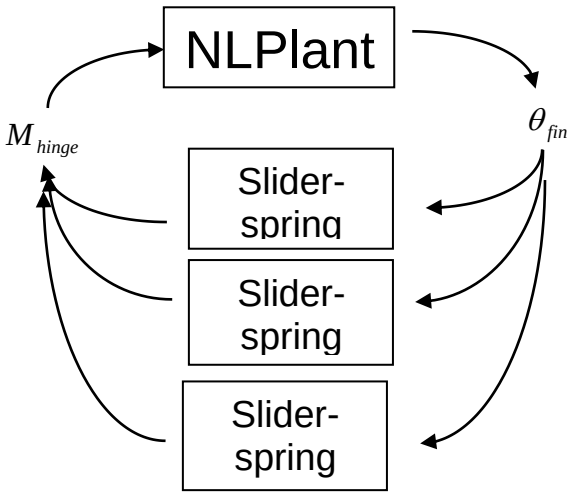

Figure 8: Block diagram of the softening NL model

2.5.3 Hysteresis + initial AoA

Since the model is linear except for the actuator model, an initial AoA would have no aeroelastic effect on the oscillation other than the effect of an initial load on the nonlinear element. This effect would be a shift in the initial conditions on the stiffness behavior. This is modeled by adding an initial displacement to the signal, and subtracting the resultant force. the block diagram of this model is presented in Figure 9.

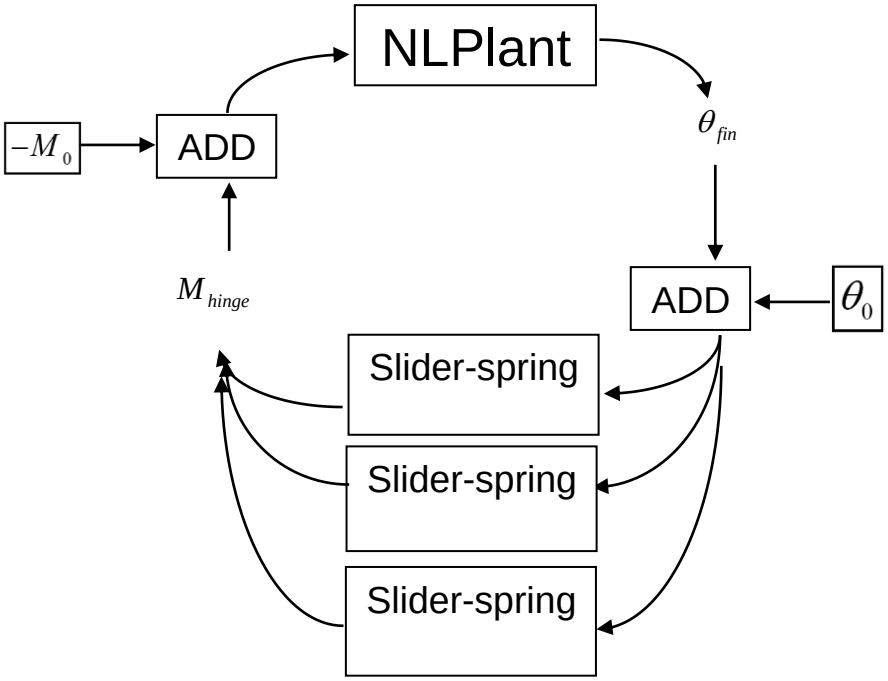

Figure 9: Block diagram of the softening NL model with initial AoA effect

3 ANALYSIS AND RESULTS

3.1 Flutter analysis to baseline model

A flutter analysis for the baseline model, (assuming the initial, high stiffness) was conducted in ZARO software, using the g method. The v-g plot obtained from the analysis is presented in Figure 10. The flutter mechanism obtained is a typical bending-torsion flutter, of the fin, where the bending mode of the fin, and the torsion mode is a “rigid” movement of the fin about its axis due to the actuator stiffness. The fin that flutters first is the one with the highest bending and the lowest torsion frequencies. For the sake of simplicity, in the non-linear studies, it was assumed that only the fluttering fin is nonlinear.

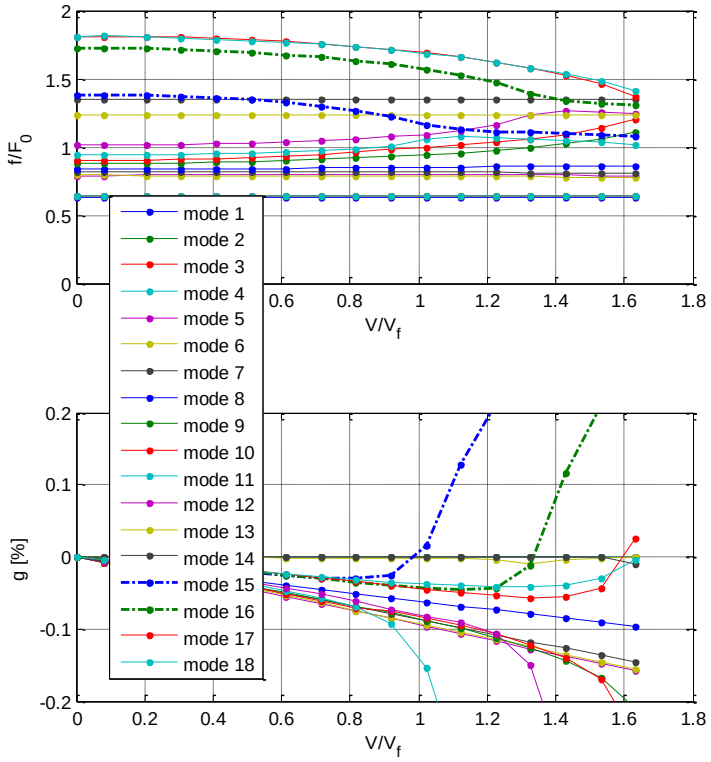

Figure 10: Flutter analysis

3.2 Response to Initial excitation

Unlike the linear analysis, where a stability analysis is conducted using the g method, in the nonlinear case, a time marching solution is required. An initial perturbation is introduced into the system in the form of an external fin moment impulse with a 1-cosine profile (using the DFORCE command). One of the main effects studied is the dependency of the response on the amplitude of the initial excitation. Although this is not the exact load history of the fin (which is characterized mainly by control commands and atmospheric turbulence), This gives an insight on the effect of the initial conditions and the excitation levels on the response. The length of the impulse is half a period of the flutter frequency. The simulation was first conducted on a linearized model, above and below the flutter boundary obtained from the g-method analysis. As expected, the solution converged below the flutter velocity and a divergent oscillation was obtained above it.

3.3 Softening only results

To “separate” the effect of the hysteresis from that of the non-linear softening the first set of simulations was conducted on a model with a nonlinear softening but without the hysteresis, based on the model described in section 2.5.1. To verify the nonlinear model, the output of the nonlinear system (i.e. the moment) is plotted as a function of the input of the nonlinear system (i.e. The fin rotation). This is presented in Figure 11,and as expected, the fits the stiffness plot of the actuator.

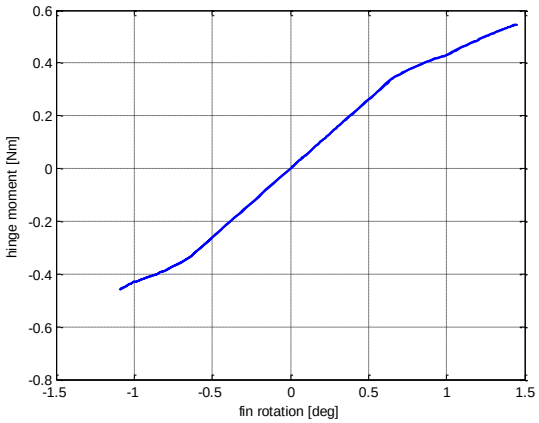

Figure 11: Hinge moment vs. fin rotation (stiffness plot obtained from analysis) softening only case

The simulation was conducted with various amplitudes of initial excitation impulse, and at various velocities below the linear flutter velocity, the system may reach a divergent oscillation, given sufficiently large IC. Therefore, flutter may occur under the linear flutter velocity. The flutter velocity as a function of the initial excitation is presented in Figure 17 in section 3.6. Sample time history results at a certain velocity, under and above the critical load, are presented in Figure 12. Similar trends were obtained in previous studied, where the softening led to earlier onset ([2][3],[4]).

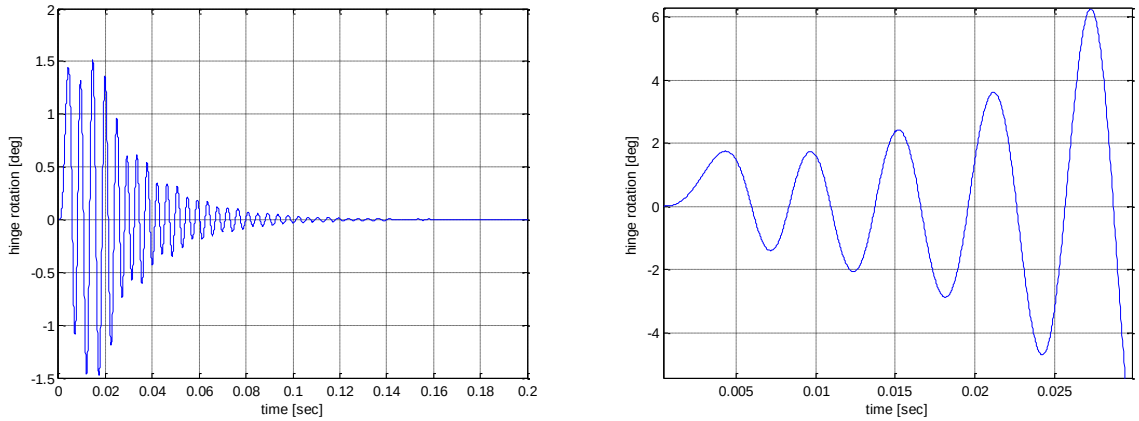

Figure 12: Time history of hinge rotations with IC below critical (left) and above critical (right), softening only case

3.4 Softening and hysteresis

Similarly, to the case of "softening only", the simulation was conducted with various amplitudes of initial excitation impulse, and at different velocities. As in the case without the hysteresis, the results showed that at a given velocity, a threshold of initial load exists, beneath which the system would converge and above which it wouldn't. The flutter velocity as a function of the initial excitation is presented in Figure 17 in section 3.6. Figure 13 presents the response of the non-linear spring, during the two analyses, at the same velocity, but with different amplitudes of initial load (above and below the threshold). The non-linear model acts as expected. The stiffness is similar to the experimental stiffness plot, and hysteresis is obtained. Note that unlike the case of "softening only", we now obtain additional dissipation due to the hysteresis. Integrating the work done over an oscillation cycle, would give us a non-zero result. Figure 14 shows the time history of the fin angle at the same two

simulations. In the converging case, several nonlinear cycles are obtained but the amplitude decreases until eventually, the system oscillates linearly, on the first branch of the stiffness plot. However, note that due to the hysteresis cycles the equilibrium point of the actuator is shifted by 0.6 degrees, which may influence the control system of the configuration. In the non-converging solution, the amplitude grows until the system is basically governed by the soft region of the stiffness plot.

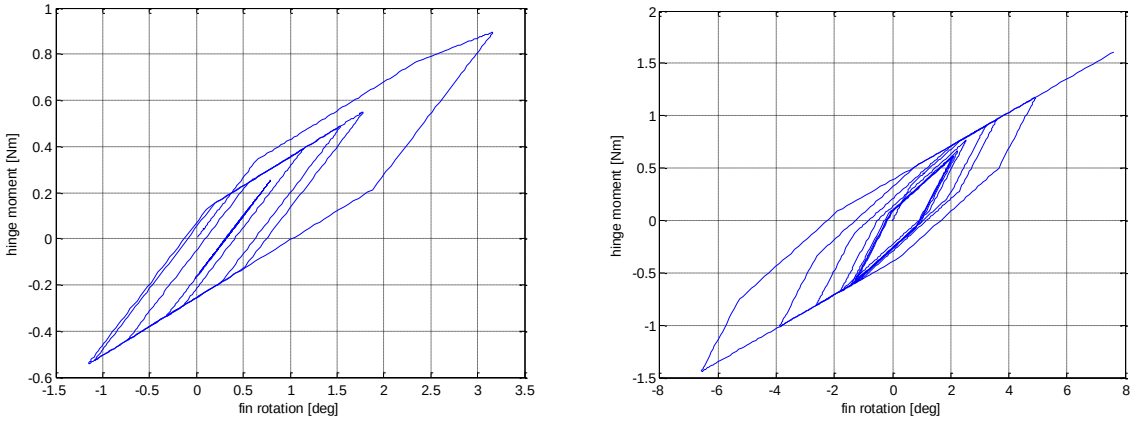

Figure 13: Hinge moment vs. fin rotation (stiffness plot obtained from analysis) with IC below critical (left) and above critical (right), hysteresis case

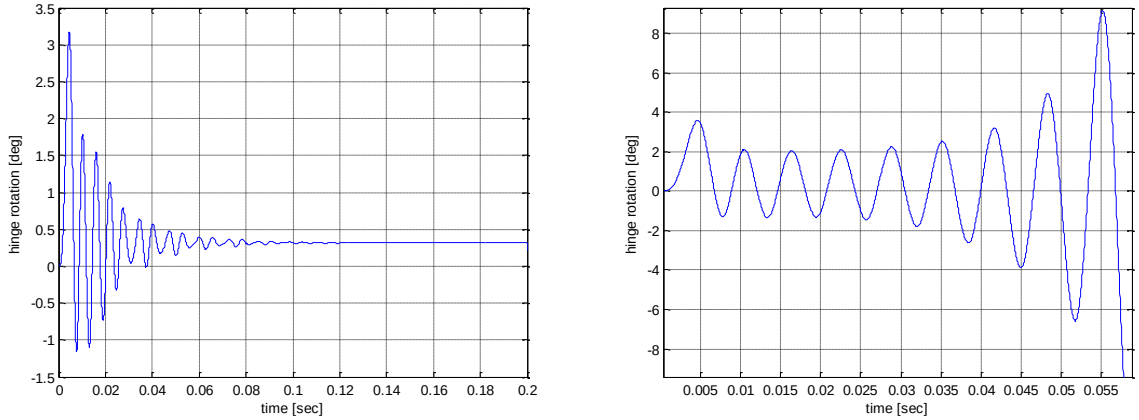

Figure 14: Time history of hinge rotations with IC below critical (left) and above critical (right) , hysteresis case

3.5 Effect of initial AoA

This case was meant to examine the effect of initial "static" load on the behavior of the system, and thus the effect of maneuver, and trim conditions. The simulations were conducted under an initial moment of 0.16 M0 and 0.8 M0 (where M0 is the maximum designed static moment of the fin). The general trend obtained in the previously studied cases is obtained in this analysis as well. At a given velocity and initial load, a threshold of initial excitation exists, above which the system cannot converge. The flutter velocity as a function of the initial excitation is presented in Figure 17. The response of the non-linear spring, during two analyses conducted at the same velocity, and initial moment, but with different initial excitation level (above and beneath stability threshold) is presented in Figure 15. Note that the results present only the addition in moment and rotation. i.e the initial moment is not seen. However, at the beginning of the analysis, the stiffness change occurs very early (at a small addition of moment) due to the initial load. Figure 16 shows the time history of the fin angle

at the same two simulations. Besides the non-symmetry of the stiffness (due to the initial load), the general behavior of the system is similar to those without initial moment.

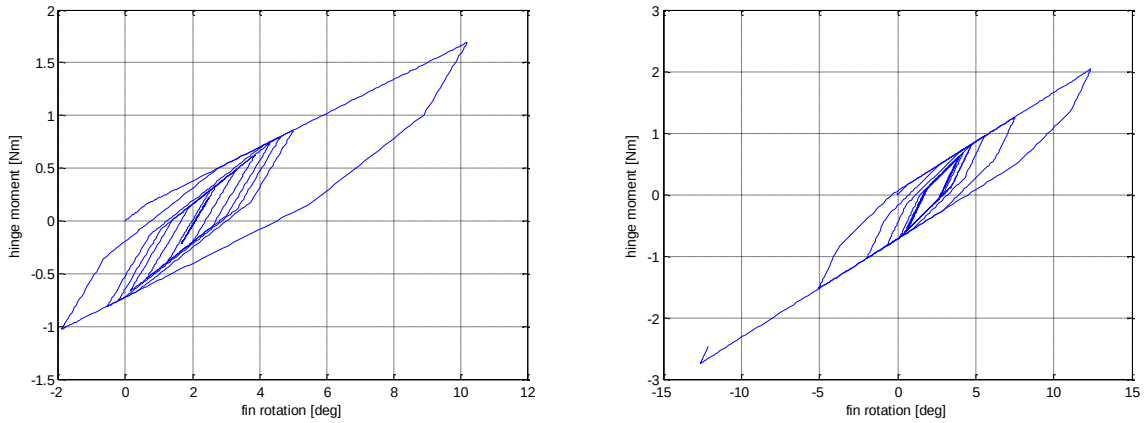

Figure 15: Hinge moment vs. fin rotation (stiffness plot obtained from analysis) with IC below critical (left) and above critical (right), hysteresis + initial AoA case

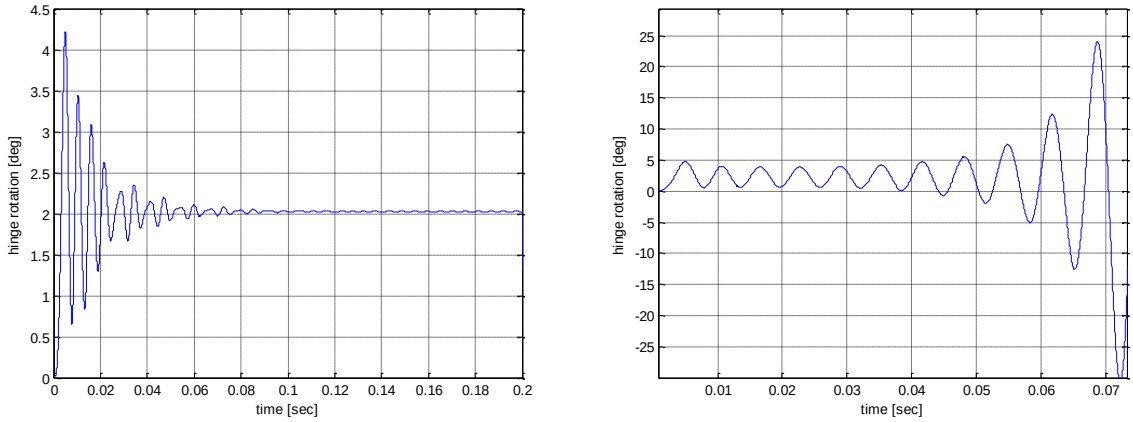

Figure 16: Time history of hinge rotations with IC below critical (left) and above critical (right), hysteresis +initial AoA case

3.6 Analysis summary

Examining Figure 17 which summarizes the results of the analyses, the following conclusions can be reached:

1. In all examined cases, no LCO was obtained.
2. The flutter velocity in all cases depends on the amplitude of the initial excitation.
3. In general, hysteresis suppresses the flutter. For a given initial excitation, the flutter velocity of the simulations including the hysteresis, is higher. This probably results from the additional energy dissipation caused by the hysteresis.
4. An initial static moment (non-symmetric initial conditions) decreases the flutter velocity. For a given initial excitation, the flutter velocity decreases with increase in the static moment. An intuitive explanation to this phenomenon can be given by the fact that under initial static moment, a smaller excitation has to be applied in order for the actuator to reach its soft region, in which the (linearized) system is unstable.

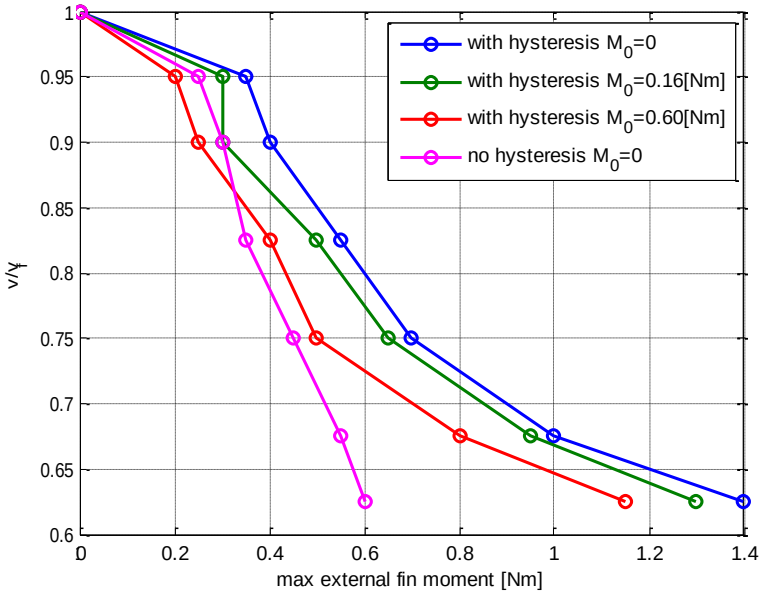

Figure 17: Flutter velocity vs. amplitude of initial perturbation in different analyses

4 EXPERIMENTAL FINDINGS

Wind tunnel tests have been conducted for the given configuration. The tests were not aimed at studying the non-linear response of the system, but rather the effects of different parameters on the systems. However, the results of a single experiment are presented here as the effect of the nonlinearity can be seen in them.

The fins were instrumented with strain gauges on the root, connected in a full Wheatstone bridge, to measure the bending moments at the root of the fins. The experiment was conducted in a constant velocity, slightly beneath the flutter speed. Once the wind tunnel was stabilized on the desired velocity, a slow delta sweep (a sweep in the fin angles) was conducted. (0.3 Hz, saw tooth). In addition to the delta sweep, the AoA was changed in the middle of the experiment. The initial excitation is obtained by the wind tunnel turbulence.

The measurements of the strain gauges are presented in Figure 18. The slow, triangle shape change in the strains indicates the change in the fin rotation (change in AoA leads to change in load on the fins and in increase in the strains). The high frequency vibrations are the elastic vibrations of the fin. The wind tunnel is turned on, and the desired velocity is reached, without stability loss. However, when the delta sweep starts, and a certain fin load is reached, the system loses stability and starts oscillating in high amplitudes, until the actuator is severely damaged. The result validates the dependency of the dynamic stability on the on the initial moment as was obtained in section 3.5, showing that indeed, a system that was stable under a given velocity and excitation loses its stability when the fin moment is increased.

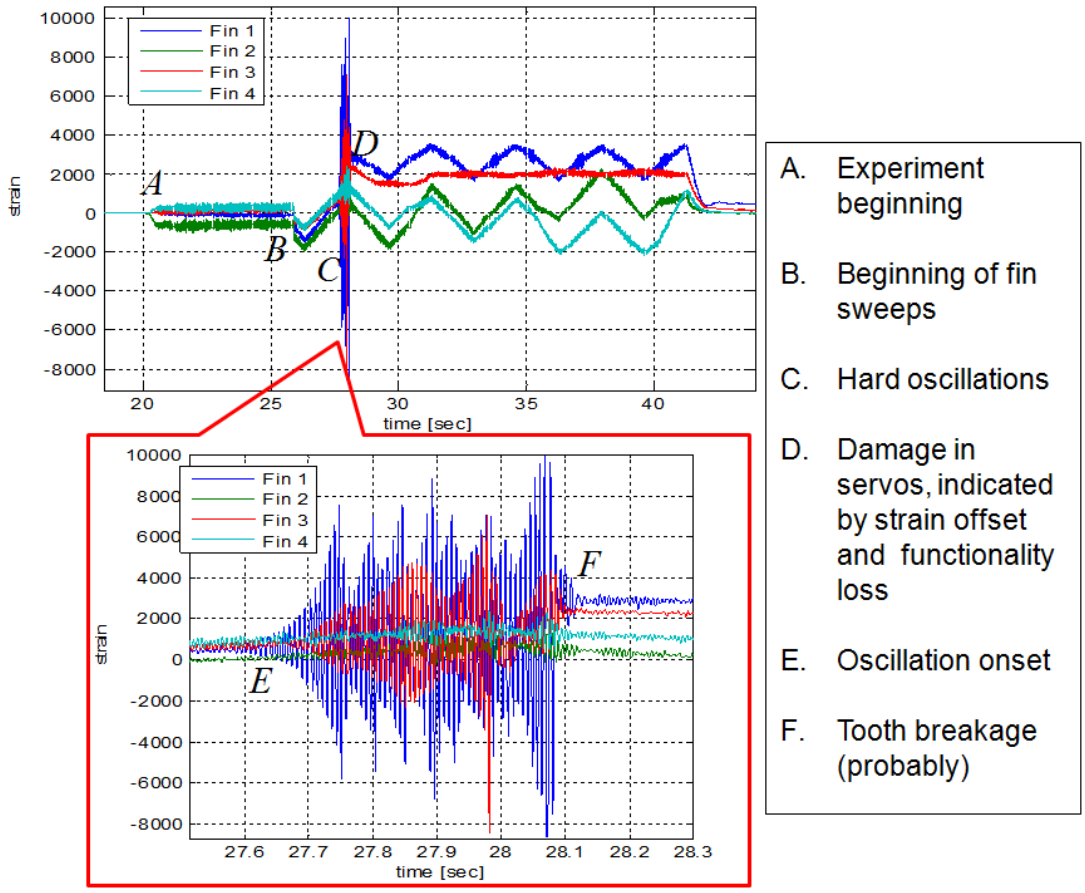

Figure 18: Strain gauge results from wind tunnel experiment

5 SUMMARY AND CONCLUSIONS

The study showed an analysis for a missile fin with nonlinearity and hysteresis in the actuator stiffness. The solution was conducted using the IOM method, implemented in the DYNRESP software. The implemented method offered a fast calculation scheme, that served for parametric studies, and multiple simulations with good accuracy and good representation of the main nonlinear effects, on one hand, and demanded little computational resources on the other hand. The nonlinearity was modeled using an incremental approach of Maxwell's slip theory.

The simulation showed that the softening nonlinearity creates a dependence of the flutter velocity on initial conditions, and high initial perturbation can lead to a lower flutter velocity than the linear flutter velocity. The hysteresis, on the other hand dampens the system, and lowers the flutter velocity, for a given initial perturbation. Finally, the effect of initial load on the fin was examined showing that an initial load on the fin decreases the flutter velocity for a given perturbation amplitude.

6 ACKNOWLEDGEMENTS

The author would like to thank Prof. Moti Karpel of Technion, Israel Institute of Technology for his guidance regarding the IOM method and some helpful discussions along the way, and his exceptional PhD student Federico Roizner for his priceless help with the DYNRESP software.

7 REFERENCES

[1] Drachinsky A. Raveh D. E. (2016) Limit-cycle oscillations of a pre-tensed membrane strip. *Journal of Fluids and Structures* 60, 1–22

[2] Patil, M.J. Hodges, D.H. Cesnik, C.E.S. (1999). Limit cycle oscillations in high-aspect-ratio wings. *AIAA Paper*-99-1464

[3] Tang D.M Dowel E.H (2004). Effects of geometric structural nonlinearity on flutter and limit cycle oscillations of high-aspect-ratio wings *Journal of Fluids and Structures,* 19 291–306

[4] Wei X. and Mottershead J. E. (2014). Aeroelastic Systems with Softening Nonlinearity, *AIAA JOURNAL* 52 (9).

[5] Xu X. Z. Gao Y.K Zhang Y. K. (2015). Aeroelastic Dynamic Response and Control og an Airfoil with Hysteresis Nonlinearity, Journal of Software Engineering, 9(2), 217-229.

[6] Luber, W. g. (1998) Flutter Prediction on a Combat Aircraft Involving Backlash on Control Surfaces. *Proceedings of the 16th International Modal Analysis Conference*, 3243, 291-299.

[7] Lacarbonara W. Cetraro M (2011). Flutter Control of a Lifting Surface via Visco-Hysteretic Vibration Absorbers, *International Journal of Aeronautical and Space Sciences,* 12 (4), 331–345

[8] Karpel, M., (2013). Dynamic Response of Nonlinear Aeroservoelastic Systems Using Increased-Order Modeling. *proceedings, 53rd Israel Annual Conference on Aerospace Sciences*

[9] Karpel M. Shousterman A. Maderuelo C. and Climent H. (2015). Dynamic Aeroservoelastic Response with Nonlinear Structural Elements. *AIAA Journal*, 53 (11) 3233-3239.

[10] Roizner F. Karpel M. Carrese R. Marzocca P. Levinski O. (2017) Towards a Hybrid Time-Frequency Domain Approach forTime-Variant Buffeting Flows. *Proceedings of 58th AIAA/ASCE/AHS/ASC Structures, Structural Dynamics, and Materials Conference, AIAA SciTech Forum, (AIAA 2017-0638)*

[11] Karpel M. Newman M. (1975). Accelerated Convergence for Vibration Modes Using the Substructure Coupling Method and Fictitious Coupling Masses, *Israel Journal of Technology*, 13. 55-62.

[12] Karpel M. and Raveh D. E.(1996). Fictitious Mass Element in Structural Dynamics. *AIAA Journal*, 34(3), 607-613.

[13] Armstrong-H´elouvry B. Dupont P. and Canudas de Wit C. (1994). A survey of models, analysis tools and compensation methods for the control of machines with friction. *Automatica*, 30 (7), 1083–1138,

COPYRIGHT STATEMENT